Acta Crystallographica Section A
Foundations and Advances
ISSN 2053-2733

Received 3 March 2014
Accepted 14 May 2014

Strain distributions and diffraction peak profiles from crystals with dislocations

Vladimir M. Kaganer[a]* and Karl K. Sabelfeld[b]

[a]Paul-Drude-Institut für Festkörperelektronik, Hausvogteiplatz 5–7, 10117 Berlin, Germany, and [b]Institute of Computational Mathematics and Mathematical Geophysics, Russian Academy of Sciences, and Novosibirsk State University, Lavrentiev prospekt 6, 630090 Novosibirsk, Russia. Correspondence e-mail: kaganer@pdi-berlin.de

Diffraction profiles for different models of dislocation arrangements are calculated directly by the Monte Carlo method and compared with the strain distributions for the same arrangements, which corresponds to the Stokes–Wilson approximation. It is shown that the strain distributions and the diffraction profiles are in close agreement as long as long-range order is absent. Analytical calculation of the strain distribution for uncorrelated defects is presented. For straight dislocations, the Stokes–Wilson and the Krivoglaz–Wilkens approximations give the same diffraction profiles, with the Gaussian central part and $\propto q^{-3}$ power law at the tails.

1. Introduction

X-ray diffraction is a well established tool for studying dislocations in crystals. Elastic fields of dislocations cause broadening of the diffraction peaks. Since elastic strain due to a dislocation decays very slowly [as $1/\rho$, where ρ is the distance from the dislocation line (see *e.g.* Landau & Lifshitz, 1970)], the entire dislocation ensemble contributes to scattering (Krivoglaz & Ryaboshapka, 1963; Wilkens, 1970*a*,*b*, 1976). This collective effect makes the problem of intensity calculation fairly complicated, even if the dislocation distribution is known. The inverse problem of retrieving the dislocation distribution from X-ray diffraction data is far more complicated. The analysis of the diffraction peak profiles from crystals with dislocations and the software developed for this purpose (Ribárik *et al.*, 2001; Scardi & Leoni, 2002; Leoni *et al.*, 2007) are based on the seminal works by Krivoglaz & Ryaboshapka (1963) and Wilkens (1970*a*,*b*, 1976), who proposed the approximate solution for straight parallel randomly located dislocations. We refer hereafter to the original papers by Krivoglaz but note that the results of these papers are also presented in his book (Krivoglaz, 1996).

The difficulty of theoretical analysis of X-ray diffraction from crystals with dislocations stems from the general formula for X-ray intensity that contains the difference between displacements $\mathbf{U}(\mathbf{r}_1) - \mathbf{U}(\mathbf{r}_2)$ in two points of the crystal. Here $\mathbf{U}(\mathbf{r})$ is the displacement field due to all dislocations in the crystal under investigation. The difference of displacements enters in a phase factor of the exponential function which is the subject of statistical average over the dislocation distribution (exact expressions are given below). This statistical average is complicated even for simple models of dislocation distributions.

Seventy years ago, Stokes & Wilson (1944) proposed a simple approximation, based on an assumption that only correlations between closely spaced points have to be taken into consideration. Then, the difference of displacements $\mathbf{U}(\mathbf{r}_1) - \mathbf{U}(\mathbf{r}_2)$ is proportional to the difference of coordinates $\mathbf{r}_1 - \mathbf{r}_2$ and the local strain at the point $\mathbf{r}_1$ (or $\mathbf{r}_2$, since they are close to each other). This approximation leads, after straightforward calculation, to a simple result, that the diffraction peak shape coincides with the strain probability distribution. Below in §2 the derivation by Stokes & Wilson (1944) is reproduced and discussed. Here it is worth noting that the approximation was proposed even before direct observation of dislocations in crystals by transmission electron microscopy and is not specific to the strain field of dislocations.

The applicability limits of the Stokes–Wilson approximation have not been established up to now. Since this approximation presumes that only local correlations are essential, one can expect that it fails when the correlations become long ranged, *i.e.* when the strain slowly varies in space. However, Leineweber & Mittemeijer (2010) have arrived at an opposite conclusion, that this approximation should be applicable when regions of practically constant strain are present.

A key step in the derivation of their seminal formula by Krivoglaz & Ryaboshapka (1963) is the approximation of the difference of displacements due to a single dislocation $\mathbf{u}(\mathbf{r}_1) - \mathbf{u}(\mathbf{r}_2)$ by the local strain multiplied with the separation $\mathbf{r}_1 - \mathbf{r}_2$. Hence, one can expect that the Stokes–Wilson approximation is valid when the Krivoglaz–Wilkens approximation is applicable, *i.e.* for random (or restrictedly random) distributions of straight parallel dislocations. On the other hand, the applicability of the Stokes–Wilson approximation is broader, since it is not restricted to straight parallel dislocations.

Present-day computing power makes feasible a direct calculation of diffraction peak profiles for given dislocation distributions. Levine & Thomson (1997), Kamminga & Delhez (2000) and Kaganer & Sabelfeld (2010) performed a statistical average over dislocation ensembles by the Monte Carlo method. These works study different arrangements of parallel straight dislocations with predefined correlations. Although a statistical average of quickly oscillating terms is required, a Monte Carlo summation is a feasible, albeit laborious, task on presently available computers. Balogh *et al.* (2012) have generated realistic three-dimensional distributions of dislocations using a discrete dislocation dynamics code. A direct Monte Carlo calculation of diffraction peak profiles was too computationally demanding, and the strain distributions were calculated instead, by employing the Stokes–Wilson approximation. The applicability of the approximation was justified by analysing the obtained peak profiles on the basis of the Krivoglaz–Wilkens theory. Upadhyay *et al.* (2014) calculated, by the Monte Carlo method, diffraction profiles for several types of dislocation distributions and compared them with the calculations in the Stokes–Wilson approximation. The best agreement is found for a three-dimensional dislocation microstructure generated by the discrete dislocation dynamics method and the worst one for a single dislocation, *i.e.* the applicability of the Stokes–Wilson approximation increases with increased disorder in the dislocation distribution.

Calculation of the strain distribution in an array of straight parallel uncorrelated dislocations can be performed by employing very general methods of statistics. Historically, the first example of a similar problem was the distribution of the electrostatic field in plasma derived by Holtsmark (1919). Further development was done by Chandrasekhar (1943) for statistics of gravitational force produced by a random distribution of stars. The distribution they found for these three-dimensional problems is close to a Gaussian distribution in the central part and possesses a power-law dependence on the tails. The central part is due to a sum of weak forces from many distant sources, while the tails arise from a few nearest sources. The probability density of the forces at the tail is $\propto f^{-9/2}$, where f is the force. The two-dimensional problem of straight dislocations is basically the same as the problem of velocity distribution from random point vortices (Chavanis & Sire, 2000) or the distribution of gravitational forces produced by rods of mass (Chavanis, 2009). It possesses a Gaussian distribution in the central part and a $\propto f^{-4}$ tail. It is also worth mentioning that the Holtsmark distribution in three dimensions belongs to the class of Levý stable distributions, while the two-dimensional case is at the border between Levý and Gaussian distributions and possesses a logarithmic divergence with the system size (Chavanis, 2009). General formulas for the strain or stress distribution due to random dislocations were derived by Strunin (1967), Zasimchuk & Selitser (1984), Groma & Bakó (1998) and Csikor & Groma (2004). The peculiar properties of the distribution were not discussed, however.

In the present paper, we perform a Monte Carlo study of the strain distributions and the diffraction peak profiles from different arrangements of dislocations, with the aim of checking the Stokes–Wilson approximation and establishing limits of its applicability. We show that the Stokes–Wilson approximation provides a good description of the diffraction profile as long as long-range order is absent. Then, we derive analytically the probability density distribution for strain caused by randomly placed straight dislocations, and compare it with the Krivoglaz (1961) results for the distribution of diffraction intensity. We find that, when the Krivoglaz–Wilkens approximation is applicable, the Stokes–Wilson approximation coincides with it. Since numerical calculation of the strain probability distribution is orders of magnitude faster than the direct calculation of the diffraction profile, the Stokes–Wilson approximation is a very useful tool to study diffraction from a broad class of dislocation distributions.

2. The Stokes–Wilson approximation

In kinematical approximation, the X-ray scattering intensity from a distorted crystal can be written as a Fourier integral

$$I(q) = \int_{-\infty}^{\infty} G(x) \exp(iqx)\, \mathrm{d}x \qquad (1)$$

of the correlation function

$$G(x) = \left\langle \exp\left\{ i\mathbf{Q} \cdot \left[\mathbf{U}(\mathbf{r}_1) - \mathbf{U}(\mathbf{r}_2) \right] \right\} \right\rangle. \qquad (2)$$

Equation (1) is written for powder diffraction and implies an average over orientations of crystallites. The coordinate x is along the reciprocal-lattice vector $\mathbf{Q}_0$. The correlations are sought between two points $\mathbf{r}_1$ and $\mathbf{r}_2$ separated by a distance x in the direction of $\mathbf{Q}_0$, and a small deviation $\mathbf{q} = \mathbf{Q} - \mathbf{Q}_0$ of the scattering vector $\mathbf{Q}$ from the reciprocal-lattice vector is also taken along $\mathbf{Q}_0$. The displacement field $\mathbf{U}(\mathbf{r})$ is the total displacement due to all defects in the crystal, and the angular brackets $\langle \ldots \rangle$ denote the statistical average over the distribution of defects. By writing infinite limits in the integral (1), we assume that the strain effect on the peak broadening dominates over the finite size and finite resolution. The account of these effects is discussed in the next section.

Our notation in equations (1) and (2) follows a standard physical notation: we denote the spatial separation by x and refer to the function $G(x)$ as the correlation function. In probability theory, the function $G(x)$ can be formulated in terms of the characteristic functional of the random strain field (Rytov *et al.*, 1988). In powder diffraction, the spatial coordinate is usually denoted by L, while the function (2) is denoted by $A_L + iB_L$ and called the Fourier transform of X-ray intensity (Warren, 1959, 1969; Leineweber & Mittemeijer, 2010). In crystallography, this function is referred to as the Patterson function.

Stokes & Wilson (1944) assume that only correlations between closely spaced points $\mathbf{r}_1$ and $\mathbf{r}_2$ play a role. Then, the difference of displacements can be approximated by the first term in the Taylor series,

$$\mathbf{Q} \cdot \left[\mathbf{U}(\mathbf{r}_1) - \mathbf{U}(\mathbf{r}_2) \right] \simeq Q\mathcal{E}x, \qquad (3)$$

where $\mathcal{E}$ is the component of the strain tensor $\hat{e}$ in the direction of the scattering vector, $\mathcal{E} = \mathbf{Q} \cdot \hat{e} \cdot \mathbf{Q}/Q^2$, and does not depend on x.

When dislocation strain is considered, the proper choice of the strain tensor needs to be discussed. Formally speaking, the gradient of the displacement field $\mathbf{U}(\mathbf{r})$ is the total strain tensor which is the sum of the elastic strain and the intrinsic strain (also called self-strain or eigenstrain). The latter quantity describes the insertion or removal of an extra half-plane when the dislocation is introduced in the crystal. The intrinsic strain is a singularity at the cut corresponding to the discontinuity of the displacement by the Burgers vector (Landau & Lifshitz, 1970). A Burgers vector is a crystal lattice vector, and the scattering vector $\mathbf{Q}$ is close to a reciprocal-lattice vector $\mathbf{Q}_0$. If a small difference between $\mathbf{Q}$ and $\mathbf{Q}_0$ is neglected here, the discontinuity of the phase factor $\mathbf{Q} \cdot \Delta\mathbf{U}$ at the cut is a multiple of 2π. Then, the intrinsic strain does not contribute to diffraction and the strain in equation (3) is the elastic strain. Upadhyay *et al.* (2014) demonstrated numerically that the calculation of the peak profile by using the difference of displacements in equation (2) and the calculation using the spatially integrated elastic strain [see equation (53) below] give the same result.

All studies that we are aware of do not distinguish between $\mathbf{Q}$ and $\mathbf{Q}_0$ in equation (2), and we also follow that line. A small additional phase factor which is neglected in such consideration is sensitive to the process of plastic deformation during the introduction of dislocations in the crystal. An investigation of its role, and the possibility of revealing the sample rheology by X-ray diffraction, requires a separate study that is beyond the scope of the present work.

By using equation (3), the statistical average in equation (2) can be written as

$$G(x) \simeq \int_{-\infty}^{\infty} P(\mathcal{E}) \exp(iQ\mathcal{E}x)\, \mathrm{d}\mathcal{E}. \tag{4}$$

Here $P(\mathcal{E})$ is the probability density distribution of the elastic strain $\mathcal{E}$. Although the approximation [equation (3)] is written for small x, we substitute equation (4) into equation (1) and perform the integration over x in the infinite limits, which gives

$$I(q) \simeq 2\pi \int_{-\infty}^{\infty} P(\mathcal{E}) \delta(q + Q\mathcal{E})\, \mathrm{d}\mathcal{E}, \tag{5}$$

where $\delta(q)$ is Dirac's delta function. Then, the X-ray diffraction profile is given by

$$I(q) \simeq 2\pi P(-q/Q), \tag{6}$$

which is the prominent result by Stokes & Wilson (1944). In the next section, we study the applicability of this approximation by Monte Carlo simulations.

3. Monte Carlo study of the strain distributions

3.1. Homogeneous dislocation distributions and short-range order

Our intention now is to calculate the probability density distributions for several representative models of the dislocation arrangements. Recently, we have calculated diffraction profiles for various models of dislocation ensembles by performing the statistical average in equation (2) by a Monte Carlo method (Kaganer & Sabelfeld, 2010). Now we calculate the probability densities for the same dislocation arrangements using the same Monte Carlo method, and compare the exact calculation of the X-ray intensity by equations (1) and (2) with the Stokes–Wilson approximation [equation (6)].

In brief, the Monte Carlo calculation is performed as follows. Dislocations are generated at random according to the model of their distribution. The total displacements $\mathbf{U}(\mathbf{r}_1)$ and $\mathbf{U}(\mathbf{r}_2)$ are calculated, due to linear elasticity, as sums of displacements from individual dislocations, for a predefined set of distances $\{x_j\}$ between points $\mathbf{r}_1$ and $\mathbf{r}_2$. The statistical average [equation (2)] is obtained by repeating the generation of dislocations. Similarly, the strain probability density is constructed as a histogram for the same dislocation configurations, using explicit expressions for the dislocation strain.

The spatial integration [equation (1)] is performed by standard quadratures. This integration strongly depends on the behaviour of the correlation function $G(x)$ at large x. Krivoglaz (1961) classified crystal lattice defects in two classes, depending on the behaviour of the correlation function $G(x)$ in the limit $x \to \infty$. For defects of the first class, the limit is a non-zero constant. It results in a delta function $\delta(q)$ in the intensity distribution, corresponding to a coherent Bragg peak. Uncorrelated dislocations belong to the second class, with a zero limit of $G(x)$ on $x \to \infty$, and the coherent Bragg peak is absent. However, the correlations between dislocations in the models considered below give rise to a non-zero limit and the coherent Bragg peak.

The distinction of the coherent and diffuse intensities is sometimes very helpful, but not necessary in the analysis of X-ray intensities. For numerical calculations, particularly in a Monte Carlo study, it is convenient to take into account the finite resolution of an experiment and evaluate both components of the intensity together, in exactly the same way as it happens in the experiment (Kaganer *et al.*, 1997; Kaganer & Sabelfeld, 2009, 2010). This is achieved by introducing a resolution function $\mathcal{R}(q)$, so that the intensity is a convolution of $I(q)$ given by equation (1) with $\mathcal{R}(q)$. Since the convolution in reciprocal space is equivalent, due to the convolution theorem, to a product in real space, the integral (1) can be rewritten as

$$I(q) = \int_{-\infty}^{\infty} G(x)R(x) \exp(iqx)\, \mathrm{d}x. \tag{7}$$

The coherence function $R(x)$ is the Fourier transform of the resolution function $\mathcal{R}(q)$. The characteristic width of $R(x)$ is referred to as the coherence length. Equation (7) allows one to avoid calculation of $G(x)$ on distances much larger than the

coherence length. For small crystallites, their sizes, rather than the coherence length, limit the integration in equation (7). In that case, the function $R(x)$ has a meaning of the crystallite size in the direction of the scattering vector. In the calculations below, we take a Gaussian function $R(x)$ and choose its width to reveal both components of the diffraction profile. In this sense, we model an experiment performed with a sufficiently good resolution.

Fig. 1(*a*) shows an example of the dislocation distribution for the model of dislocation distribution that we have proposed recently (Kaganer & Sabelfeld, 2010). In this model, the screening of the long-range strain fields of dislocations is achieved by generating pairs of dislocations with opposite Burgers vectors. The position of the centre of a pair, the orientation of the vector connecting two dislocations in a pair, and the distance between two dislocations in a pair are random. The diffraction profiles in Figs. 1(*b*), 1(*c*) are calculated for the exponential distribution of the distances between dislocations in the pairs. The mean distance between dislocations in the pairs is the screening radius R_c. We use the mean distance between dislocations $r_d = n^{-1/2}$, where n is the dislocation density, as unit length. Then, the screening distance R_c coincides with the Wilkens' parameter $M = R_c/r_d$ (Wilkens, 1970*a*). As long as $R_c \geq 1$, the pairs overlap, rather than form dipoles. The dislocation distribution shown in Fig. 1(*a*) is generated for $R_c = 1$. Even in this case of rather little overlap of the pairs, one cannot distinguish separate pairs in the distribution.

The diffraction profiles calculated by the Monte Carlo method using equations (1) and (2) have been presented in our previous publication (Kaganer & Sabelfeld, 2010). They are shown in Figs. 1(*b*), 1(*c*) by thick grey lines. The two plots show the same diffraction profiles in logarithmic and linear scale, respectively. The probability density distributions of strain are calculated by the Monte Carlo method for the same model of dislocation distribution and presented in Figs. 1(*b*), 1(*c*) by thin red lines. We note here that each pair of curves is plotted without introducing an arbitrary scale factor that would bring the curves to the same scale: the factor 2π from equation (6) is used. A good agreement between exact calculation and the Stokes–Wilson approximation for $R_c \geq 1$ is evident.

Figs. 1(*d*)–1(*f*) present Monte Carlo calculations of the diffraction profiles for the Wilkens' restrictedly random dislocation distribution, also taken from our previous publication cited above. In this model, the crystal is divided into cells (shown in Fig. 1*d* by thin grey lines), each cell containing randomly distributed dislocations. The total number of dislocations in each cell is the same, and the numbers of dislocations with opposite Burgers vectors are equal in each cell. We found that, in the case of one pair of dislocations per cell, our previous calculation (Kaganer & Sabelfeld, 2010) did not perform a sufficient average, so that Figs. 1(*e*), 1(*f*) present an improved calculation. In the same way as above, the full Monte Carlo calculation by equations (1) and (2) is shown by thick grey lines, while the strain density distribution is presented by thin red lines. In the case of one pair of dislocations per cell, the exact calculation shows a resolution-limited central peak, which is absent in the strain distribution. This peak is studied further in the next sections. With the increasing number of dislocation pairs per cell, the agreement between the calculated peak profiles and the Stokes–Wilson approximation improves.

Figs. 2(*a*), 2(*c*) present an example of the dislocation arrangement and the diffraction profiles for edge dislocations, also taken from Kaganer & Sabelfeld (2010). The dislocation pairs are purposely 'polarized', in terms of Groma *et al.* (1988), Ungár *et al.* (1989) and Groma & Monnet (2002). One can see in Fig. 2(*a*) that all dislocation pairs are of vacancy type, meaning that a segment of the half-plane is taken out between two dislocations in a pair. As a result, the peak profiles are asymmetric. As the mean distance between dislocations in the pair increases, the peak shifts in the negative direction of q. The peak profiles obtained in our previous Monte Carlo calculation (thick grey lines) are in good agreement also with the strain probability distribution in this case. The asymmetry and the shift of the peaks are reproduced by the Stokes–Wilson approximation.

With the aim of testing the Stokes–Wilson approximation on a spatially inhomogeneous system, we consider

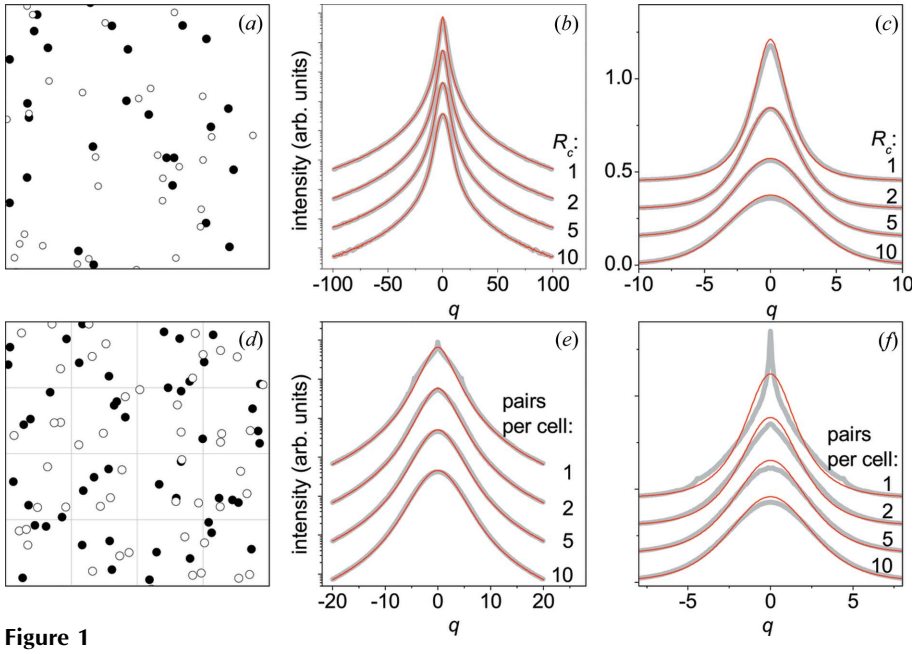

Figure 1
Dislocation arrangements (left) and diffraction profiles in logarithmic (middle) and linear (right) scales for (*a*)–(*c*) randomly distributed pairs of screw dislocations and (*d*)–(*f*) Wilkens' restrictedly random dislocation distribution. Both diffraction peak profiles (thick grey lines) and strain probability distributions (thin red lines) are calculated by the Monte Carlo method.

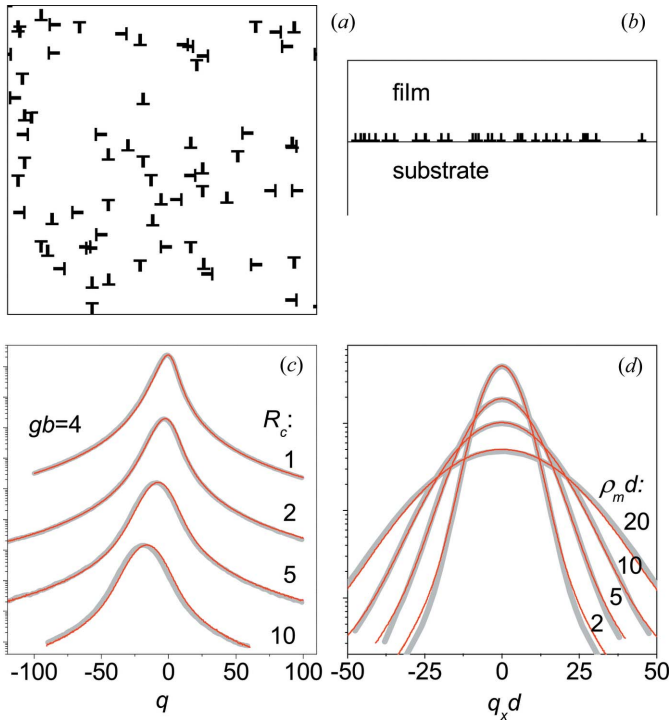

Figure 2
Dislocation arrangements (top) and diffraction profiles (bottom) for (*a*), (*c*) randomly distributed pairs of edge dislocations and (*b*), (*d*) uncorrelated misfit dislocations at the film–substrate interface. Both diffraction peak profiles (thick grey lines) and strain probability distributions (thin red lines) are calculated by the Monte Carlo method.

diffraction peaks from the misfit dislocations at the interface between a substrate and an epitaxic film with the lattice spacing different from that of the substrate. The results of our Monte Carlo study (Kaganer & Sabelfeld, 2009) are presented in Figs. 2(*b*), 2(*d*). Since the misfit dislocations are located in the plane of the interface, their density $\rho_{\rm m}$ is the number of dislocations per unit length along the line perpendicular to the dislocation lines, *i.e.* it is a *linear density*. That contrasts with the bulk dislocation density, which is the *areal density*. The dimensionless parameter characterizing diffraction peaks is the product $\rho_{\rm m}d$, where d is the film thickness.

The epitaxic films are studied in a triple-crystal diffraction setup with an analyser crystal. Equation (1) presumes the powder average and is not applicable in this case. Rather, the intensity distribution is written as (Kaganer *et al.*, 1997):

$$I(q_x, q_z) = \int_{-\infty}^{\infty} {\rm d}x \int_0^d \int_0^d {\rm d}z_1\, {\rm d}z_2 G(x, z_1, z_2) \times \exp\left[iq_x x + iq_z(z_1 - z_2)\right], \quad (8)$$

where the x axis is in the plane of the interface and the z axis is normal to it, and the points $\mathbf{r}_1$ and $\mathbf{r}_2$ in equation (2) are separated by the distance x in the plane of the interface. Since the system is not translationally invariant in the direction of the film normal, the z coordinates of these two points enter equation (8) separately. Equation (3) has to be modified by expanding over small distances x and $\zeta = z_1 - z_2$. We restrict ourselves to the symmetric Bragg reflections (diffraction vector $\mathbf{Q}$ is directed along the z axis). Then, $\mathbf{Q}\cdot\mathbf{U} = QU_z$ and two components of distortions, $\mathcal{E}_{zx} = \partial U_z/\partial x$ and $\mathcal{E}_{zz} = \partial U_z/\partial z$, have to be taken into consideration. They depend on the coordinate $z = (z_1 + z_2)/2$ in the film, since a translational invariance in this direction is absent. Then, instead of equation (3), we have

$$\mathbf{Q}\cdot\left[\mathbf{U}(\mathbf{r}_1) - \mathbf{U}(\mathbf{r}_2)\right] \simeq Q\mathcal{E}_{zx}(z)x + Q\mathcal{E}_{zz}(z)\zeta, \quad (9)$$

and the Stokes–Wilson approximation is

$$I(q_x, q_z) \simeq (2\pi)^2 \int_0^d P_{zx}(-q_x/Q, z)P_{zz}(-q_z/Q, z)\,{\rm d}z, \quad (10)$$

where $P_{zx}(\mathcal{E}_{zx}, z)$ is the probability distribution of the distortion component $\mathcal{E}_{zx}$ at a distance z from the surface ($0 < z < d$). The probability distribution P_{zz} is defined similarly. The integration is performed over the film thickness.

Fig. 2(*d*) compares the results of the Monte Carlo calculation of the diffraction profiles for uncorrelated misfit dislocations performed by Kaganer & Sabelfeld (2009) (thick grey lines) with the Monte Carlo calculation by equation (10) for the same dislocation distributions (thin red lines). Different curves correspond to different densities of misfit dislocations. A good agreement between the exact calculation and the Stokes–Wilson approximation is also reached in this case of spatially inhomogeneous dislocation distribution.

3.2. Inhomogeneous dislocation distributions and long-range order

The results presented in Figs. 1 and 2 demonstrate that the Stokes–Wilson approximation is applicable for different models of dislocation distributions and in a wide range of parameters. Our aim now is to establish the limits of its applicability. For this purpose, we modify the models discussed above to bring them in parameter ranges where the Stokes–Wilson approximation no longer agrees with the calculated peak profiles.

In Fig. 3, the model of the strain field screening by arranging dislocations in pairs (see Fig. 1*a*) is investigated for smaller mean distances $R_{\rm c}$ between dislocations in the pairs. Fig. 3(*a*) presents an example of the distribution of pairs of screw dislocations with opposite Burgers vectors, with the mean distance between dislocation in pairs $R_{\rm c} = 0.25$ (we remind readers that the distances are measured in units of the mean distance between all dislocations in the system). In this case, the dislocation dipoles can be recognized in the distribution. For $R_{\rm c} < 1$, the diffraction profiles in Figs. 3(*b*), 3(*c*) possess sharp Bragg peaks in the centre of the diffraction profile. This central peak is a manifestation of the long-range order. The resolution function is shown by the dashed line, demonstrating that the peak is resolution limited. The Stokes–Wilson approximation, which assumes only short-range correlations, obviously cannot catch this peak.

The behaviour of $G(x)$ at large x can be established by considering the limit $x \to \infty$ in equation (2). Since displacements in two points $\mathbf{r}_1$ and $\mathbf{r}_2$ are not correlated in the limit of large separations, we have

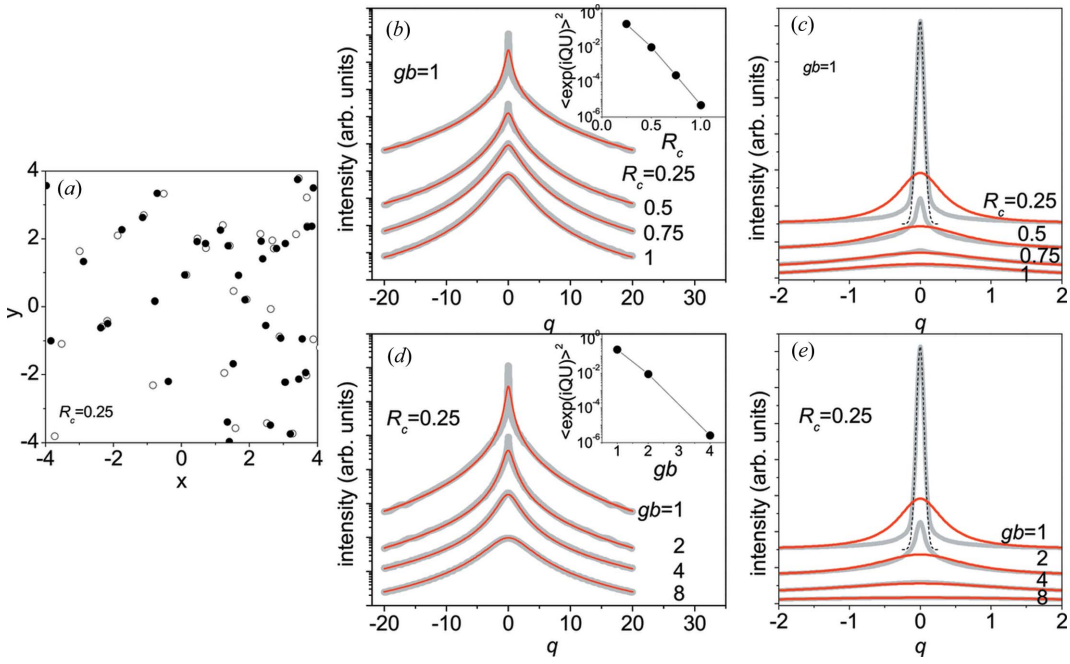

Figure 3
(*a*) An example of an arrangement of the randomly placed and randomly oriented dipoles of screw dislocations ($R_c = 0.25$), (*b*), (*c*) diffraction peak profiles calculated for dislocation distributions with different screening distances R_c and (*d*), (*e*) diffraction peak profiles in different reflection orders. Monte Carlo calculation of the diffraction profiles is shown by thick grey lines, and the strain probability distributions by thin red lines. The middle and the right columns present the same peaks on different scales. The insets in (*b*) and (*d*) show calculated Debye–Waller factors $\langle \exp(i\mathbf{Q}\cdot\mathbf{U})\rangle^2$. Dashed lines in (*c*), (*e*) show the resolution function.

$$G(x \to \infty) = \langle \exp[i\mathbf{Q}\cdot\mathbf{U}(\mathbf{r})]\rangle^2. \quad (11)$$

This is the static Debye–Waller factor which determines the coherent Bragg intensity in equation (1) $I_{\rm coh}(q) = 2\pi \exp(-2W)\delta(q)$, where it is denoted

$$\exp(-W) = \langle \exp[i\mathbf{Q}\cdot\mathbf{U}(\mathbf{r})]\rangle. \quad (12)$$

Since we do not consider the thermal Debye–Waller factor in the present paper, we refer below to the static Debye–Waller factor as simply the Debye–Waller factor. The inset in Fig. 3(*b*) presents the Debye–Waller factors calculated by the Monte Carlo method.

Formally, the arrangement of dislocations in pairs and the screening of the long-range strain field of a dislocation by surrounding dislocations results in a finite Debye–Waller factor for any screening radius R_c. However, the Debye–Waller factor quickly decreases with the increasing R_c and the coherent peak is not practically visible. To observe it, one would need an unreasonably high resolution (and a large crystal size). Figs. 3(*b*), 3(*c*) show that the coherent peak is not visible and the Stokes–Wilson approximation is applicable when the Debye–Waller factor $\exp(-2W) < 10^{-3}$.

Since the Debye–Waller factor quickly decreases with the reflection order, the Stokes–Wilson approximation can be applicable for the higher-order reflections, even if it fails to describe the low-order ones. The calculations presented in Figs. 3(*b*), 3(*c*) are performed for the first reflection order, $gb = 1$ (here it is denoted $gb = \mathbf{Q}\cdot\mathbf{b}/2\pi$). In Figs. 3(*d*), 3(*e*), we study the case of dislocation dipoles with $R_c = 0.25$, now in different reflection orders. A comparison of the Monte Carlo calculation of the diffraction profiles (thick grey lines) with the probability distribution for the dislocation strain (thin red lines) shows that the accuracy of the Stokes–Wilson approximation increases with the increasing reflection order. We note that, according to equation (6), one and the same probability distribution, but with the abscissa scaled by gb, is used for all curves. From the Debye–Waller factors presented in the inset to Fig. 3(*d*), we arrive at the same conclusion, that the Stokes–Wilson approximation can be used when the Debye–Waller factor $\exp(-2W) < 10^{-3}$.

A small Debye–Waller factor does not mean that the X-ray intensity is small: it only indicates that the coherent peak is weak and the intensity is transferred to the diffuse peak. These diffuse peaks are the Bragg peaks observed experimentally for crystals with dislocations (Krivoglaz, 1996). In the framework of kinematical theory and in the absence of absorption, the total integrated intensity is preserved and only redistributes (see further discussion in §4.6).

Our next model is a modification of the Wilkens' restrictedly random dislocation distribution. In the dislocation distribution shown in Fig. 4(*a*), the sample is divided in cells of equal area, the cells are seeded with randomly placed dislocations and the total Burgers vector in each cell is zero. However, in contrast with the Wilkens' distribution, only a fraction $f < 1$ of the cells is filled, while other cells remain empty. Fig. 4(*a*) shows an example of the dislocation distribution when a fraction $f = 0.25$ of the cells is filled. With decreasing f, the distribution becomes less homogeneous. Accordingly, the Debye–Waller factor increases, the correlation function $G(x)$ in Fig. 4(*b*) tends to a larger limiting value

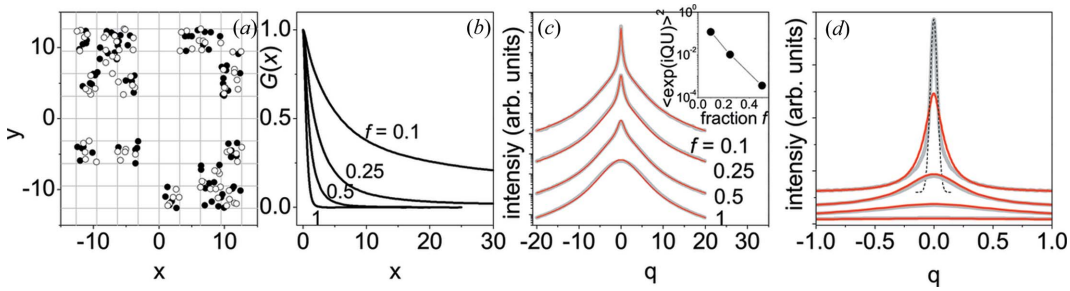

Figure 4
(*a*) An example of dislocation distribution in the rarefied Wilkens model. There are five dislocation pairs per cell, and a fraction $f = 0.25$ of cells is filled. (*b*) Correlation functions $G(x)$ for different fractions f of filled cells. (*c*) Diffraction profiles calculated from these correlation functions (thick grey lines) and the strain probability distributions (thin red lines). The inset shows calculated Debye–Waller factors $\langle \exp(i\mathbf{Q}\cdot\mathbf{U})\rangle^2$. (*d*) The central part of the diffraction profiles in (*c*) shown in linear scale. The dashed line represents the resolution function.

at $x \to \infty$, and the diffraction profiles in Figs. 4(*c*), 4(*d*) acquire sharp coherent peaks at $q = 0$. The resolution function shown in Fig. 4(*d*) by the dashed line demonstrates that this peak is resolution limited. A comparison of the Monte Carlo calculation of the diffraction peaks (thick grey lines) with the strain probability density distribution (thin red lines) shows that the accuracy of the Stokes–Wilson approximation increases as the Debye–Waller factor decreases below 10^{-3}.

Fig. 5 demonstrates the effect of the increasing ordering in the distribution of misfit dislocations. The dislocations are generated as a Markov chain with the probability density of the distances between subsequent dislocations given by a gamma distribution (Kaganer & Sabelfeld, 2009). The use of a gamma distribution, with its only parameter γ controlling the order, allows one to proceed from completely random dislocations at $\gamma = 1$ (exponential distribution) to almost periodic dislocations at $\gamma \gg 1$. Fig. 5(*a*) shows examples of dislocation distributions with different degrees of order. Thick grey lines in Fig. 5(*b*) are the corresponding diffraction profiles. As the positional order of dislocations is improved, the satellite reflections appear and become sharper with increasing γ. Calculation in the Stokes–Wilson approximation by equation (10) is shown by thin red lines and agrees with the diffraction profiles as long as the coherent Bragg peak is absent.

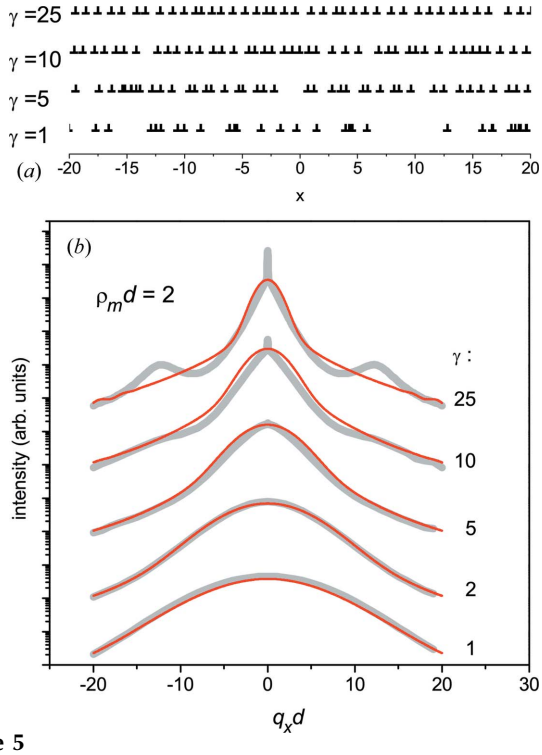

Figure 5
(*a*) Examples of the misfit dislocation arrangements generated as Markov chains with the gamma distribution for distances between dislocations. (*b*) Diffraction peak profiles calculated for these dislocation distributions (thick grey lines) and corresponding strain probability distributions (thin red lines).

4. Strain distributions and peak profiles from random dislocations

4.1. The central limit theorem

Thin red lines in Figs. 1–4 show the probability density distributions of elastic strain due to various dislocation arrangements, obtained by Monte Carlo calculations. They are far from a Gaussian shape suggested by the Warren & Averbach (1950, 1952) approximation. The central parts of the distributions have a Gaussian shape, but their tails follow the q^{-3} power law. Such distributions are exactly what is expected when a sum of a large, but finite, number of independent random variables is considered (Sornette, 2006).

The central limit theorem states that the probability density distribution of a sum of a large number of independent random variables converges to the Gaussian distribution. Strain in a crystal with random dislocations is a sum of strains due to individual dislocations and, due to a slow decay of strain with distance, a large number of dislocations contribute to strain in each point of a crystal. However, the applicability conditions of the theorem have to be taken into consideration.

First, the dispersion of the variables is required to be finite. As discussed below, this condition is satisfied when the dislocation strain is screened, particularly in our model of overlapping dislocation pairs, or in Wilkens' restrictedly random dislocation distribution. For random dislocation distribution, the dispersion logarithmically diverges with the system size. The logarithmic divergence puts the distribution on the border between Gaussian and Levý distributions for

which also an extended central limit theorem holds (Chavanis, 2009).

When the dislocation strain is screened and the dispersion is finite, the central limit theorem states that the Gaussian distribution is approached as the number of terms in the sum giving comparable contributions tends to infinity. Since distant dislocations are screened, it means that the Gaussian distribution is approached when the dislocation density tends to infinity. The convergence to the Gaussian distribution need not necessarily be the same for different parts of the distribution. For a large but finite dislocation density, the Gaussian law is a good description of the central part of the distribution. This central part is formed as a result of comparable contributions of many dislocations to the total strain. In contrast, the tails of the distribution arise due to a strong strain in the vicinity of a single dislocation, while other dislocations provide negligibly small contributions. Such convergence to the Gaussian law with the increasing number of random variables, fast in the centre of the distribution and slow at its tails, is described by Sornette (2006) in detail. Below we derive the probability density distribution for strain due to dislocations and find that it follows these general laws. The distribution is Gaussian in the central part and has the algebraic (with the power -3) tails.

4.2. Strain distribution

The aim of the present section is to derive a general expression for the probability density distribution analytically. We follow the method developed for other systems with random sources of fields (Holtsmark, 1919; Chandrasekhar, 1943; Chavanis & Sire, 2000; Chavanis, 2009).

Let us consider N parallel dislocations randomly placed in a cylinder of radius R; the dislocation density is $n = N/\pi R^2$. We consider both the limit $N \to \infty$ in the Krivoglaz & Ryaboshapka (1963) analysis of random dislocation distribution, and the case of finite N in the Wilkens (1970*a*,*b*, 1976) model of restrictedly random distribution. We refer to dislocations as strain sources, but the results remain valid for any other randomly distributed defects. In particular, we consider also random pairs of opposite dislocations in our model of screening of the long-range strains due to surrounding dislocations. Then, the strain field of a dislocation pair is used instead of the strain due to a single dislocation. The only assumption is the absence of correlations in positions of defects under consideration.

The strain $\mathcal{E}$ is, due to linear elasticity, a sum of strains produced by all dislocations,

$$\mathcal{E} = \sum_{i=1}^{N} \varepsilon_i. \tag{13}$$

The probability density $P(\mathcal{E})$ can be written as

$$P(\mathcal{E}) = \int \delta\left(\mathcal{E} - \sum_{i=1}^{N} \varepsilon_i\right) \prod_{i=1}^{N} p(\boldsymbol{\rho}_i)\, \mathrm{d}\boldsymbol{\rho}_i, \tag{14}$$

where $\boldsymbol{\rho}_i$ are two-dimensional vectors in the plane perpendicular to dislocation lines and $p(\boldsymbol{\rho}_i)\,\mathrm{d}\boldsymbol{\rho}_i$ is the probability of occurrence of the ith dislocation at $\boldsymbol{\rho}_i$.

The delta function can be represented by its Fourier transform,

$$\delta(\mathcal{E}) = \frac{1}{2\pi} \int_{-\infty}^{\infty} \exp(-i\mathcal{E}\xi)\, \mathrm{d}\xi. \tag{15}$$

Then, $P(\mathcal{E})$ becomes

$$P(\mathcal{E}) = \frac{1}{2\pi} \int_{-\infty}^{\infty} \exp(-i\mathcal{E}\xi)\tilde{P}(\xi)\, \mathrm{d}\xi, \tag{16}$$

where $\tilde{P}(\xi)$ is equal to

$$\tilde{P}(\xi) = \left(\int_{|\boldsymbol{\rho}|=0}^{R} \exp[i\varepsilon(\boldsymbol{\rho})\xi] p(\boldsymbol{\rho})\, \mathrm{d}\boldsymbol{\rho} \right)^N. \tag{17}$$

Since dislocations are uniformly distributed, $p(\boldsymbol{\rho}) = 1/\pi R^2$. We also take into account that

$$\frac{1}{\pi R^2} \int_{|\boldsymbol{\rho}|=0}^{R} \mathrm{d}\boldsymbol{\rho} = 1 \tag{18}$$

and rewrite equation (17) as

$$\tilde{P}(\xi) = \left(1 - \frac{1}{\pi R^2} \int_{|\boldsymbol{\rho}|=0}^{R} \left\{1 - \exp[i\varepsilon(\boldsymbol{\rho})\xi]\right\} \mathrm{d}\boldsymbol{\rho} \right)^N. \tag{19}$$

Let us define

$$T(\xi) = n \int_{|\boldsymbol{\rho}|=0}^{R} \left\{1 - \exp[i\varepsilon(\boldsymbol{\rho})\xi]\right\} \mathrm{d}\boldsymbol{\rho} \tag{20}$$

and rewrite equation (19) as

$$\tilde{P}(\xi) = \left[1 - \frac{T(\xi)}{N} \right]^N. \tag{21}$$

The convergence of the integral (20) as $R \to \infty$ depends on the screening of the dislocation strains at large distances. The strain due to a single dislocation possesses a universal dependence $\varepsilon(\boldsymbol{\rho}) \propto \rho^{-1}$ on the distance. Then, for uncorrelated dislocations, the integral (20) diverges at the upper limit as $\ln R$. This integral is explicitly calculated below in §4.4 for screw dislocations. For our model of dislocation screening by uncorrelated pairs of dislocations with opposite Burgers vectors, equation (20) can be applied by taking the strain field of a dislocation pair as $\varepsilon(\boldsymbol{\rho})$. At distances exceeding the separation in the pair, the strain field of a pair is that of a dislocation dipole, $\varepsilon(\boldsymbol{\rho}) \propto \rho^{-2}$, and the integral (20) converges at large distances. Similarly, in the Wilkens' restrictedly random distribution, the strain from a cell containing equal numbers of the dislocations with opposite Burgers vectors

decays as $\varepsilon(\boldsymbol{\rho}) \propto \rho^{-2}$ on the distances exceeding the cell size, and the integral (20) converges.

In the case of screened dislocations, $T(\xi)$ does not depend on N in the limit $N \to \infty$ and equation (21) gives

$$\tilde{P}(\xi) = \exp[-T(\xi)]. \tag{22}$$

For unscreened dislocations, equation (22) is not a true limit at $N \to \infty$ but remains valid as long as $T(\xi) \ll N$. This latter restriction is not important, however. The Fourier integral (16) is governed by the behaviour of the function $T(\xi)$ in the range $T(\xi) \lesssim 1$. When $T(\xi)$ becomes large, its contribution to $\tilde{P}(\xi)$ is negligible, irrespective of the use of either equation (21) or (22).

If several types of dislocations are present, a generalization of equation (22) is straightforward. Since dislocations of different types are not correlated to each other, the strain probability is a product of probabilities due to different types of dislocations. Then, equation (20) is replaced by a sum

$$T(\xi) = \sum_{\alpha} n_{\alpha} \int\limits_{|\boldsymbol{\rho}|=0}^{R} \left\{1 - \exp[i\varepsilon_{\alpha}(\boldsymbol{\rho})\xi]\right\} \mathrm{d}\boldsymbol{\rho}, \tag{23}$$

where α denotes the types of dislocations, and n_{α} and $\varepsilon_{\alpha}(\boldsymbol{\rho})$ are the density and the strain field of dislocations of corresponding type, respectively. In particular, if dislocations with opposite Burgers vectors are present with equal densities, equation (23) simplifies to

$$T(\xi) = n \int\limits_{|\boldsymbol{\rho}|=0}^{R} \left\{1 - \cos[\varepsilon(\boldsymbol{\rho})\xi]\right\} \mathrm{d}\boldsymbol{\rho}. \tag{24}$$

Equations (13)–(24) provide a general solution for strain distribution from any defects, described by their strain $\varepsilon(\boldsymbol{\rho})$. Before proceeding to further analysis specific to the dislocation strain field, let us derive in the same way a general expression for the X-ray intensity distribution.

4.3. Intensity distribution

The X-ray intensity distribution is given by equation (1) as the Fourier transform of the correlation function $G(x)$. Let us now perform, by the same method as used in the previous section for the strain distribution, a direct statistical average of the correlation function (2). We refer, as above, to dislocations as random uncorrelated defects. However, the results are applicable to any other random uncorrelated defects, particularly dislocation pairs in our model of the dislocation screening. We consider N dislocations in a cylinder of radius R, with the dislocation density $n = N/\pi R^2$. The total displacement $\mathbf{U}(\mathbf{r})$ is, due to linear elasticity, a sum of displacements due to individual dislocations,

$$\mathbf{U}(\mathbf{r}) = \sum_{i=1}^{N} \mathbf{u}(\mathbf{r} - \boldsymbol{\rho}_i), \tag{25}$$

where the position of the ith dislocation is given by a two-dimensional vector $\boldsymbol{\rho}_i$ in the plane perpendicular to dislocation lines.

The statistical average (2) can be written as

$$G(x) = \int \exp\left\{ i \sum_{j=1}^{N} \left[\mathbf{Q} \cdot \mathbf{u}(\mathbf{r}_1 - \boldsymbol{\rho}_j) - \mathbf{Q} \cdot \mathbf{u}(\mathbf{r}_2 - \boldsymbol{\rho}_j)\right] \right\} \times \prod_{j=1}^{N} p(\boldsymbol{\rho}_j)\, \mathrm{d}\boldsymbol{\rho}_j. \tag{26}$$

Since dislocations are uniformly distributed, $p_j(\boldsymbol{\rho}) = 1/\pi R^2$ and

$$G(x) = \left(\frac{1}{\pi R^2} \int\limits_{|\boldsymbol{\rho}|=0}^{R} \exp\left\{ i\left[\mathbf{Q} \cdot \mathbf{u}(\mathbf{r}_1 - \boldsymbol{\rho}) - \mathbf{Q} \cdot \mathbf{u}(\mathbf{r}_2 - \boldsymbol{\rho})\right]\right\} \mathrm{d}\boldsymbol{\rho} \right)^{N}. \tag{27}$$

Using equation (18), the latter formula can be written as

$$G(x) = \left[1 - \frac{\mathcal{T}(x)}{N}\right]^{N}, \tag{28}$$

where

$$\mathcal{T}(x) = n \int\limits_{|\boldsymbol{\rho}|=0}^{R} \left(1 - \exp\left\{ i\left[\mathbf{Q} \cdot \mathbf{u}(\mathbf{r}_1 - \boldsymbol{\rho}) - \mathbf{Q} \cdot \mathbf{u}(\mathbf{r}_2 - \boldsymbol{\rho})\right]\right\}\right) \mathrm{d}\boldsymbol{\rho}. \tag{29}$$

We remind readers that, because of the powder average, the points $\mathbf{r}_1$ and $\mathbf{r}_2$ are separated by a distance x in the direction of diffraction vector $\mathbf{Q}$. In a general case, the function $\mathcal{T}(\mathbf{r}_1, \mathbf{r}_2)$ has to be considered. As long as $\mathcal{T}(x) \ll N$, equation (28) can be written as

$$G(x) = \exp[-\mathcal{T}(x)]. \tag{30}$$

Equations (29), (30) are the main general result for X-ray intensity distribution from uncorrelated defects by Krivoglaz (1961, 1996). We have derived these equations in a way that is different from his original derivation.

As a first step in their calculation of the diffraction peak profiles from crystals with dislocations, Krivoglaz & Ryaboshapka (1963) find that the main contribution to the integral (29) is due to distant dislocations, *i.e.* the distance $|\mathbf{r}_1 - \mathbf{r}_2|$ between points $\mathbf{r}_1$ and $\mathbf{r}_2$ is small compared with the distance $|\boldsymbol{\rho}|$ between this pair of points and the dislocation line. Then, they expand the difference of displacements in equation (29) in a Taylor series,

$$\mathbf{Q} \cdot \mathbf{u}(\mathbf{r}_1 - \boldsymbol{\rho}) - \mathbf{Q} \cdot \mathbf{u}(\mathbf{r}_2 - \boldsymbol{\rho}) \simeq \mathbf{Q} \cdot \partial\mathbf{u}/\partial\mathbf{r} \cdot (\mathbf{r}_1 - \mathbf{r}_2), \tag{31}$$

where $\partial\mathbf{u}/\partial\mathbf{r}$ denotes the distortion tensor with the components $\partial u_i/\partial r_j$. The result coincides with equation (20). One can see that the approximation (31) is the same as the approximation (3) in the derivation of the Stokes & Wilson (1944) approximation. Thus, for uncorrelated dislocations, the Krivoglaz & Ryaboshapka (1963) calculation of the diffraction profiles from crystals with dislocations involves the same approximations as the Stokes & Wilson (1944) approximation of the diffraction profile by strain distribution, and differs only in the sequence of approximations. Further analysis in the next section is equally applicable for both of them.

4.4. Strain distribution for screw dislocations

4.4.1. Uncorrelated dislocations. Let us perform now a detailed calculation for the renowned problem of screw dislocations. We consider, as above, N dislocations in a cylinder of radius R, with an equal number of dislocations with opposite Burgers vectors. Thus, the results are applicable for a random dislocation distribution by Krivoglaz & Ryaboshapka (1963) in the limit $N \to \infty$, and for a restrictedly random dislocation distribution by Wilkens (1970*a*,*b*, 1976) if N and R are kept finite. The strain field of a screw dislocation is $\varepsilon(\boldsymbol{\rho}) = b\cos\varphi/2\pi\rho$, where the polar coordinates (ρ, φ) are used for the two-dimensional vector $\boldsymbol{\rho}$. The integral (24) becomes

$$T(\xi) = n\int_0^R \rho\,\mathrm{d}\rho \int_0^{2\pi} \mathrm{d}\varphi\big\{1 - \cos[b\xi\cos\varphi/2\pi\rho]\big\}. \qquad (32)$$

Let us introduce a new variable $y = b\xi/2\pi\rho$ and make use of the equality

$$\int_0^{2\pi} \cos(y\cos\varphi)\,\mathrm{d}\varphi = 2\pi J_0(y), \qquad (33)$$

where $J_0(y)$ is the Bessel function. Then, equation (32) transforms to

$$T(\xi) = \frac{nb^2\xi^2}{2\pi} \int_{b\xi/2\pi R}^{\infty} \big[1 - J_0(y)\big]\,\frac{\mathrm{d}y}{y^3}. \qquad (34)$$

Let us define

$$\eta = b\xi/2\pi R \qquad (35)$$

and introduce a function

$$f(\eta) = 4\int_{\eta}^{\infty} \big[1 - J_0(y)\big]\,\frac{\mathrm{d}y}{y^3}. \qquad (36)$$

For $\eta \ll 1$, the main contribution to the integral (36) is from the region of small y. Using the expansion $J_0(y) \simeq 1 - y^2/4$, we find $f(\eta) \simeq -\ln\eta$. In the opposite limit $\eta \gg 1$, the Bessel function in the integrand can be neglected compared to 1, which gives $f(\eta) \simeq 2/\eta^2$. Since equation (34) can be written as

$$T(\xi) = \frac{1}{2}N\eta^2 f(\eta), \qquad (37)$$

we find that the condition $T(\xi) \ll N$, which is required to proceed from equation (20) to equation (22), is satisfied for $\eta \lesssim 1$. However, as discussed in §4.2, the contribution from large η is exponentially small anyway. The use of equation (37) in the whole range of η allows a smooth calculation of the Fourier integral (16).

Fig. 6 compares the function $f(\eta)$ given by equation (36) with the respective bulky formula proposed by Wilkens (1970*b*). Both functions have the same $f(\eta) \simeq -\ln\eta$ behaviour at $\eta \ll 1$. Krivoglaz & Ryaboshapka (1963) arrived at equation (37) in another way, by expanding the cosine term in equation (24) for small arguments. From an estimate of the remaining terms, they concluded that the applicability of the approximation $f(\eta) \simeq -\ln\eta$ is limited by the condition $\ln N \gg 1$.

The dashed line in Fig. 6 shows a function $-\ln\eta + 1$. It is a good approximation of the function $f(\eta)$ in the whole range $\eta \lesssim 1$. Thus, the applicability condition by Krivoglaz & Ryaboshapka (1963) is formally correct, since the correction to $-\ln\eta$ is of the order of 1. However, the correction is constant, so that the function can be represented as $-\ln(\eta/e)$, where e is the base of the natural logarithm. By comparing with the definition of η in equation (35), one can see that the approximation $f(\eta) \simeq -\ln\eta$ can be preserved by using eR instead of R. In an analysis of experimental data, the screening radius R is not known in advance and considered as a fit parameter. A difference between R and eR cannot be revealed. In the Monte Carlo simulations, the correlation radius R_c taken on input and the cutoff radius R, obtained by the fit of the diffraction profile, do not coincide (Kaganer & Sabelfeld, 2010). The latter depends also on the distribution of dislocations modelled in the Monte Carlo calculation. We note that e as a correction factor appears for screw dislocations and for a particular model of their distribution. Other dislocation distributions give rise to other numerical values of the correction constant.

Thus, the approximation $f(\eta) \simeq -\ln\eta$ makes sense in the whole range $\eta \lesssim 1$, with an appropriate correction of the radius R. However, the use of this approximation in the Fourier integration (16) gives rise to unphysical oscillations caused by a rigid cut of the integration range. An advantage of the Wilkens' function $f(\eta)$, or the one given by equation (36), is the possibility of smoothly extending the Fourier integration over ξ to infinite limits. We also plot in Fig. 6 the function $f(\eta) = -\ln[\eta/(\eta + e)]$, which has the same behaviour at $\eta \ll 1$ and was suggested by Kaganer *et al.* (2005) with a pragmatic purpose of providing a smooth calculation of the Fourier integral in infinite limits. Any of these functions can equally well be used in the diffraction profile calculations.

4.4.2. Pairs of dislocations. Consider now the model of randomly positioned pairs of dislocations with opposite Burgers vectors. The distance between dislocations in the pairs R_c is a screening distance. Here we take, for simplicity, the same distance R_c for all pairs. This unimodal distribution is

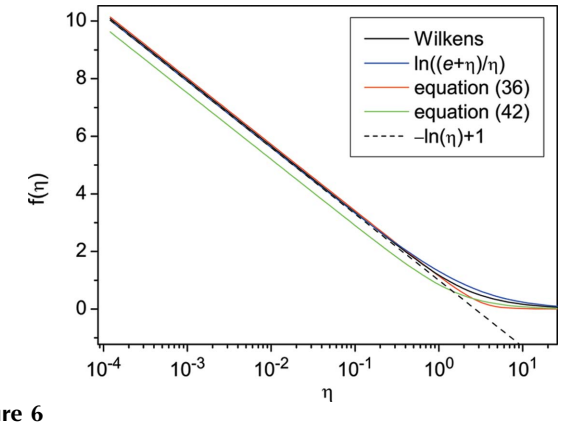

Figure 6
The function $f(\eta)$ for different models of dislocation distributions.

one of the distributions considered by Kaganer & Sabelfeld (2010), and it has been shown that the results for different distributions of R_c are very similar. A generalization of the equations below to any other distribution of R_c is straightforward and requires an additional integration over the distribution.

The strain field of a screw dislocation located at the origin is

$$\frac{b}{2\pi R_c}\frac{y}{x^2+y^2}, \tag{38}$$

where we use dimensionless Cartesian coordinates $\boldsymbol{\rho}/R_c = (x, y)$. Then, the strain field of a pair of dislocations with opposite Burgers vectors, separated by the distance R_c, is

$$\varepsilon(\boldsymbol{\rho}) = \frac{b}{2\pi R_c}F(x, y), \tag{39}$$

with the definition

$$F(x, y) = \left[\frac{y}{\left(x-\frac{1}{2}\right)^2+y^2} - \frac{y}{\left(x+\frac{1}{2}\right)^2+y^2}\right] \tag{40}$$

and x axis chosen along the line connecting two dislocations in the pair.

As discussed above, equation (24) for dislocation pairs can be written in infinite limits. Substituting strain [equation (40)], we can represent this equation as

$$T(\xi) = \frac{1}{2}N_c\eta^2 f(\eta), \tag{41}$$

with the definition

$$f(\eta) = \frac{1}{\pi\eta^2}\int_{-\infty}^{\infty}\int_{-\infty}^{\infty}\left\{1-\cos[\eta F(x, y)]\right\}\mathrm{d}x\,\mathrm{d}y \tag{42}$$

and $N_c = \pi R_c^2 n$ is the average number of dislocations in a cylinder of radius R_c. When using equation (24), we take into account that the density of dislocation pairs is $n/2$.

The function $f(\eta)$ given by equation (42) is also shown in Fig. 6. It possesses the same behaviour as other functions on this plot and differs only by the constant that has to be used for correction of the $-\ln\eta$ function. The use of another correction constant again stresses that this constant is not universal. In all other respects, all functions shown in Fig. 6 can be used for analysis of experiments equally well. For this reason, we do not distinguish between these functions, denoting all of them by $f(\eta)$.

4.5. Shape of diffraction peaks

We have found above that, for random straight dislocations, the intensity distribution in the Krivoglaz–Wilkens approximation coincides with the strain density distribution. To be explicit, on substitution $\xi = -Qx$ the correlation function $G(x)$ in the Krivoglaz–Wilkens approximation is identical with the function $\tilde{P}(\xi)$. Let us use more common terms of the intensity distribution to describe both distributions. This intensity distribution was analysed in many works, and we recollect here its main features. We collect equations (6), (16), (22), (37), and represent the correlation function (2) in the form

$$G(x) = \exp[-T(x)], \tag{43}$$

where

$$T(x) = \frac{\pi}{2}n(gb)^2x^2 f(gbx/2\pi R). \tag{44}$$

The numerical factor $\pi/2$ in equation (44) is for screw dislocations. In a general case, this factor, which is also called 'the contrast factor', is a well defined quantity whose proper value is needed for accurate dislocation density determination. It was calculated for different crystal symmetries, anisotropies and dislocation arrangements in a number of papers. We refer to the most recent publication (Martinez-Garcia *et al.*, 2009) that also reviews previous works.

The central part of the diffraction peak is Gaussian, since at small q a weak x-dependence of the logarithmic term $f(gbx/2\pi R) \simeq \ln(2\pi R/gbx)$ does not play a role. In the logarithmic term, one can substitute $x = n^{-1/2}/gb$. Then, the logarithmic term is equal to $\frac{1}{2}\ln(4\pi N)$, where $N = \pi R^2 n$ is the number of dislocations within the correlation radius. This radius is a crystal size in the Krivoglaz treatment, the size of the cells in the Wilkens model, or the mean separation of dislocations in the pairs in our model of the dislocation screening. Thus, the central part of the peak is a Gaussian,

$$I(q) = \left[\frac{4}{n(gb)^2\ln(4\pi N)}\right]^{1/2}\exp\left[-\frac{q^2}{\pi n(gb)^2\ln(4\pi N)}\right]. \tag{45}$$

The intensity distribution at q which is large compared to the half-width of the Gaussian is governed by the behaviour of $G(x)$ at small x. For small x, one has $T(x) \ll 1$ and hence $\exp[-T(x)] \simeq 1 - T(x)$. Comparing with equation (21) at $N = 1$, we find that $I(q)$ at large q is the strain density distribution in a cylinder containing a single dislocation. This strain distribution can be calculated directly (Wilson, 1955).

When the sum of strains [equation (13)] is dominated by one term, the correlation function is

$$G(x) = N\int_{|\boldsymbol{\rho}|=0}^{R}\exp[iQ\varepsilon(\boldsymbol{\rho})x]p(\boldsymbol{\rho})\,\mathrm{d}\boldsymbol{\rho}. \tag{46}$$

Substituting into equation (1) and integrating over x first, we get

$$I(q) = 2\pi n\int_{|\boldsymbol{\rho}|=0}^{R}\delta[q + Q\varepsilon(\boldsymbol{\rho})]\,\mathrm{d}\boldsymbol{\rho}. \tag{47}$$

For the strain field of a screw dislocation, we have $Q\varepsilon(\boldsymbol{\rho}) = gb\cos\varphi/\rho$ and integration of the delta function gives

$$I(q) = 2\pi^2\frac{n(gb)^2}{q^3}. \tag{48}$$

The q^{-3} asymptotic law at large q is well established (Wilson, 1955; Wilkens, 1963, 1970*a*; Groma & Bakó, 1998; Groma, 1998; Kaganer *et al.*, 2005).

Thus, both the strain probability distribution and the diffraction profile have a Gaussian central part and an alge-

braic tail. The Gaussian part is due to small strains from a large number of dislocations, while the algebraic tail is due to the vicinity of a single dislocation. The transition region between these parts is determined by equating the corresponding expressions (45) and (48).

4.6. Debye–Waller factor

As we have already discussed in §3.2 above, a non-zero limit of the correlation function $G(x \to \infty)$ is a manifestation of the long-range order which gives rise to a coherent Bragg peak. This peak is a delta function $\delta(q)$ in an infinite crystal illuminated by a plane wave, or a sharp peak with the width determined by either the crystal size or the X-ray coherence in a realistic case. Let us compare the total integrated intensity of the diffraction peak

$$J_{\rm tot} = \int\limits_{-\infty}^{\infty} I(q)\,{\rm d}q \tag{49}$$

with that of its coherent part $J_{\rm coh}$. Substituting equation (2) into equation (1), we get $J_{\rm tot} = 2\pi G(x = 0)$. In the same way, the integrated intensity of the coherent peak is $J_{\rm coh} = 2\pi G(x \to \infty)$. Since $G(x = 0) = 1$ and, according to equation (11), $G(x \to \infty) = \exp(-2W)$, we have

$$J_{\rm coh}/J_{\rm tot} = \exp(-2W). \tag{50}$$

It may be worth noting here that, in the framework of the kinematical theory and in the absence of the X-ray absorption, the integrated intensity (49) does not depend on the dislocation density or dislocation correlations. An increase of the dislocation density or, more generally, an increase of disorder causes a redistribution of the X-ray intensity from the coherent peak to the diffuse peak. The Debye–Waller factor becomes small and the coherent peak is not seen, unless the resolution is extremely high. In this respect, Bragg peaks observed from crystals with dislocations are diffuse peaks (Krivoglaz, 1996).

A statistical average in equation (12) is performed in the same way as it is done above for the strain distribution, and gives

$$W = n \int\limits_{|\boldsymbol{\rho}|=0}^{R} \left\{1 - \cos[\mathbf{Q}\cdot\mathbf{u}(\boldsymbol{\rho})]\right\} {\rm d}\boldsymbol{\rho}. \tag{51}$$

For uncorrelated screw dislocations, one has $\mathbf{Q}\cdot\mathbf{u}(\boldsymbol{\rho}) = gb\varphi$, where $\varphi = \arctan(y/x)$ is the polar angle. The cosine term in equation (51) is zero after the angular integration over φ, and the Debye–Waller exponent is $W = \pi R^2 n = N$. In the limit $N \to \infty$, the intensity of the coherent peak is zero. For the restrictedly random dislocation distribution, the number N of the dislocations in a cell is finite, and formally the coherent peak is present. However, since its intensity is proportional to $\exp(-2N)$, this peak can be revealed only for small N. This is demonstrated in Fig. 1(*f*), where the central resolution limited peak is visible only in the top curves. Note that the number of dislocation pairs indicated in the figure is $N/2$, half of the number of dislocations.

For our model of dislocation pairs, the displacement $\mathbf{u}(\boldsymbol{\rho})$ in equation (51) is that of a pair of dislocations with opposite Burgers vectors. At distances much larger than the separation between dislocations in the pair $R_{\rm c}$, a Taylor series expansion gives $\mathbf{Q}\cdot\mathbf{u}(\boldsymbol{\rho}) \simeq QR_{\rm c}\varepsilon(\boldsymbol{\rho})$, where $\varepsilon(\boldsymbol{\rho})$ is the strain due to a single dislocation. Then, the calculation is the same as in §4.4.1 and the Debye–Waller exponent W is equal to $T(\xi)$ in equations (32)–(37) with $\xi = QR_{\rm c}$, and hence $\eta = gbR_{\rm c}/R$. For the system size that is large compared to the dislocation distances in the pairs, $R \gg R_{\rm c}$, the Debye–Waller exponent can be written, using equation (37), as

$$W = \frac{\pi}{2}(gb)^2 nR_{\rm c}^2 \ln(R/gbR_{\rm c}). \tag{52}$$

It logarithmically diverges with the system size. Then, the Debye–Waller factor algebraically depends on the system size, $\exp(-2W) \propto R^{-\beta}$, where $\beta = \pi(gb)^2 nR_{\rm c}^2$. Hence, the Debye–Waller factors calculated by the Monte Carlo method and plotted in the insets of Figs. 3(*b*), 3(*c*) are not fully correct. They are calculated for system sizes several hundred times larger than the mean distance between dislocations, and their size dependence was not studied. Equation (52) shows that the Debye–Waller factor quickly decreases as either the screening distance $R_{\rm c}$ or the reflection order increases. Hence, in accordance with the Monte Carlo calculations in §3, the coherent Bragg peak can be revealed only for small screening distances and in low-order reflections. The Stokes–Wilson approximation becomes applicable for higher-order reflections, even if it is not applicable for low orders.

4.7. Probability density of the spatially averaged strain

The statistical average in equation (2) is performed over the probability density distributions of the difference of displacements $\mathbf{U}(\mathbf{r}_1) - \mathbf{U}(\mathbf{r}_2)$ for all distances x between points $\mathbf{r}_1 - \mathbf{r}_2$. Instead of the approximate equation (3) valid only for small x, one can write an equality

$$\mathbf{Q}\cdot\left[\mathbf{U}(\mathbf{r}_1) - \mathbf{U}(\mathbf{r}_2)\right] = Q\overline{\mathcal{E}}_x x, \tag{53}$$

thus introducing the spatially averaged strain

$$\overline{\mathcal{E}}_x = \frac{1}{x}\int\limits_0^x \mathcal{E}\,{\rm d}x. \tag{54}$$

Here the bar denotes the spatial average, so that $\overline{\mathcal{E}}_x$ is a random quantity representing the average over a distance x of the strain $\mathcal{E}$ due to randomly placed dislocations. This quantity is widely discussed in the literature (McKeehan & Warren, 1953; Warren, 1959, 1969; Leineweber & Mittemeijer, 2010; Balogh *et al.*, 2012; Upadhyay *et al.*, 2014).

Let us denote by $P_x(\overline{\mathcal{E}}_x)$ its probability density. Then, equation (2) can be written as

$$G(x) = \int\limits_{-\infty}^{\infty} \exp(iQ\xi x) P_x(\xi)\,{\rm d}\xi. \tag{55}$$

As we have already discussed in §2, the strain $\mathcal{E}$ in equation (3) is the elastic strain. Accordingly, equations (53) and (54) treat the dislocation displacement field as a continuous multi-

valued function, rather than a single-valued function possessing a discontinuity. The two representations of the dislocation displacement field lead to the same result when the exponential function in equation (2) is used, but to different results when equations (53), (54) are employed. The displacement field of a straight dislocation contains a term with $\arctan(y/x)$, which provides the displacement by Burgers vector when making a closed contour around the dislocation line. In the Monte Carlo calculations presented below, we use the Fortran function `atan2(y, x)` in the integration along the x direction. This function has a discontinuity at the negative x axis which is not crossed. The use of a formally equivalent function $-$`atan2(x, y)` gives the wrong result, since the discontinuity of this latter function on the y axis is crossed in the integration along x.

Fig. 7 presents Monte Carlo calculations of the probability density distributions $P_x(\overline{\mathcal{E}}_x)$ for different distances x. They are calculated in the same manner as $P(\mathcal{E})$, but as histograms of $\mathbf{Q}\cdot[\mathbf{U}(\mathbf{r}_1)-\mathbf{U}(\mathbf{r}_2)]/x$. The dislocation distributions are the ones presented in Figs. 1(a) and 3(a): pairs of screw dislocations with opposite Burgers vectors have random uncorrelated positions and orientations, the distance between dislocations in the pairs follows the exponential distribution with the mean distance between dislocations in the pairs R_c. Fig. 7 shows the probability distributions for the case of strongly overlapping pairs, with the mean distance $R_c = 5$ larger than the mean distance between dislocations in the system (taken as the length unit). One and the same curves are shown in the figure in three different scales, to reveal different parts of the distributions. The strain is presented in the units of

$$\mathcal{E}_0 = bn^{1/2}/2\pi. \tag{56}$$

As a numerical example, for a Burgers vector $b = 0.3$ nm and a mean distance between dislocations $n^{-1/2} = 100$ nm, one has $\mathcal{E}_0 \simeq 5\times10^{-4}$.

The probability density distribution at $x \to 0$, shown by a thick black line, is the one used in the Stokes–Wilson approximation. It is studied above in detail and plotted in Figs. 1–4 by thin red lines. It is Gaussian in the central part, see Fig. 7(a), and possesses the ξ^{-3} power law at the tails, see Fig. 7(b). In the opposite limit $x \gg 1$, the whole probability distribution is Gaussian, since the displacements $\mathbf{U}(\mathbf{r}_1)$ and $\mathbf{U}(\mathbf{r}_2)$ are decorrelated and the central limit theorem is applicable. The transition from one limit to the other proceeds in a quite peculiar way. The width of the central Gaussian part of the distribution does not notably change as long as $x \leq 1$. The ξ^{-3} power law also persists up to some x-dependent value of strain, and then the probability abruptly drops down. Similar distributions, combining two notably different regions, were found in the study of the velocity difference in a system of random vortices (Min *et al.*, 1996).

Thick lines in Fig. 8 present the correlation functions $G(x)$ obtained by a direct Monte Carlo calculation using equation (2) (Kaganer & Sabelfeld, 2010). We also calculated these correlation functions using equation (55) with the probability density distributions $P_x(\overline{\mathcal{E}}_x)$ from Fig. 7, and found that these two calculations agree fully with each other. Thin lines in Fig. 8 present the Stokes–Wilson approximation given by equation (4), *i.e.* by using the probability density distribution at $x \to 0$ in the integral (55) instead of the whole set of the distributions for different x. The Stokes–Wilson approximation agrees with the direct calculation of the correlation function as long as $R_c \geq 1$, but notably deviates from it for small R_c. In this latter case, the correlation function tends to a finite value in the limit $x \to \infty$ reflecting the long-range order, while the Stokes–Wilson approximation probes the local strain and does not

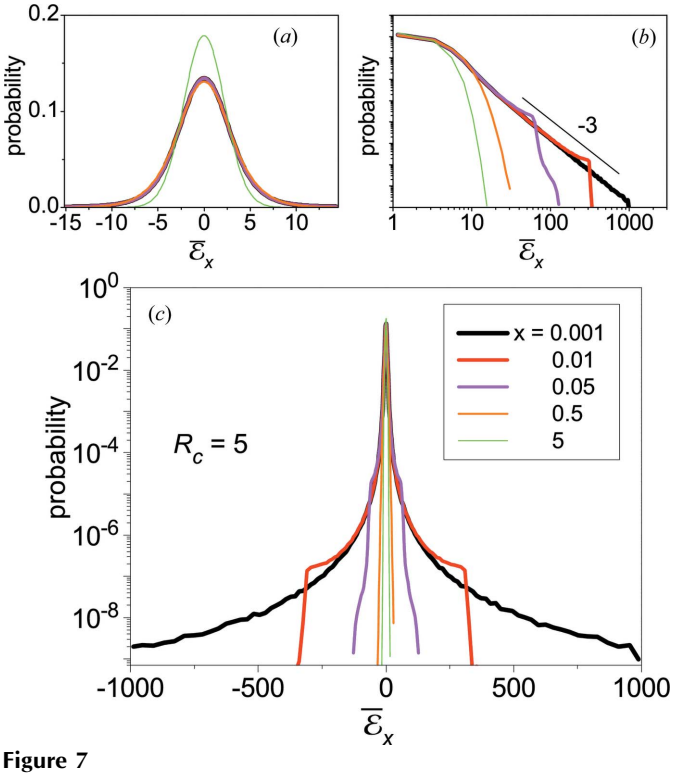

Figure 7
Monte Carlo calculation of the probability density distributions of spatially averaged strain $\overline{\mathcal{E}}_x$ for different distances x. The model of random uncorrelated dislocation pairs with the exponential distribution of the distances between dislocations, the mean distance in the pairs $R_c = 5$ (all distances are in the units of the mean distance between dislocations $n^{-1/2}$).

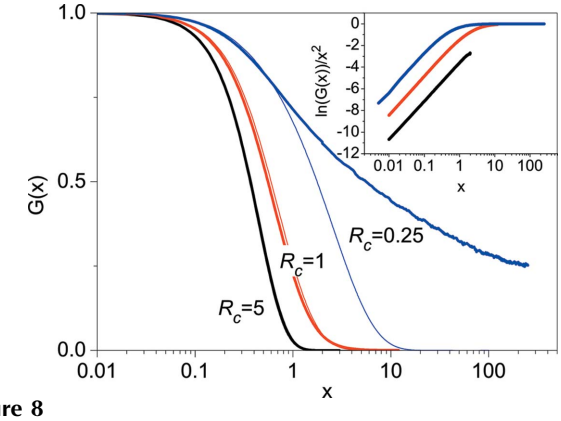

Figure 8
Correlation functions $G(x)$ calculated by the Monte Carlo method: the direct calculation by equation (2) (thick lines) and in the Stokes–Wilson approximation by equation (4).

catch the long-range order. The two curves still coincide for $x \leq 1$. As a result, on Fourier transformation (1) from the correlation function $G(x)$ to the intensity distribution $I(q)$, the tails of the curve at $q > 1$ are described by the Stokes–Wilson approximation, but the central part of the distribution is not. Since the limit $G(x \rightarrow \infty)$ is equal to the Debye–Waller factor $\exp(-2W)$, we find, in agreement with the analysis of the previous sections, that the Stokes–Wilson approximation describes the whole intensity distribution when the Debye–Waller factor is zero or negligibly small, and fails when the Debye–Waller factor increases. Fig. 8 is a real-space presentation of the same behaviour as described in the reciprocal-space representation in the previous sections.

To reveal the behaviour of the correlation function $G(x)$ at small x, the inset in Fig. 8 shows the same functions as in the main plot, calculated by the Monte Carlo method, and presents the x dependence of $\ln[G(x)]/x^2$. One can see that for $x \leq 1$, the curves follow the $\ln[G(x)]/x^2 \propto \ln x$ dependence given by equations (43), (44). This plot explicitly shows that the Warren & Averbach (1950, 1952) approximation does not take into account the logarithmic dependence in the function $f(\eta)$.

5. Conclusions

We have performed Monte Carlo simulations for different models of distributions of straight dislocations and found that the diffraction profiles and the strain probability distributions are very close to each other. In other words, the Stokes–Wilson approximation has a broad applicability range. Numerical calculation of the strain probability distribution is several orders of magnitude faster, since it does not involve an average of oscillating terms needed in a direct calculation of the peak profile. The strain probability distribution can be an effective way of diffraction profile calculation for more complicated dislocation distributions, for which direct calculation is too computationally demanding.

Numerical and analytical calculations of the strain probability distributions of dislocations show that the distributions have a Gaussian shape only in the central part of small strain. This central part is due to contributions of many surrounding dislocations. The tails are due to large strain from a single closest dislocation and follow a power law.

For straight dislocations, the Stokes–Wilson approximation has the same applicability range as the Krivoglaz–Wilkens formula, and gives the same result. They are both described by Fourier transform of the correlation function, obtained by Krivoglaz & Ryaboshapka (1963) and Wilkens (1970*a*,*b*, 1976), which has a structure $G(x) \sim \exp(-x^2 \ln x)$ (here all constants are omitted and only the structure of the expression is shown). It is the term $\ln x$ in the exponent that gives rise to the algebraic tails of the profiles. However, for smooth calculation of the Fourier integral in the whole range of x, this term needs to be modified. Besides the Wilkens' function $f(\eta)$ used for this purpose, we have proposed and plotted in Fig. 6 three other functions which can equally well be used instead.

We purposely modified the models of dislocation distributions to find the limits of the applicability of the Stokes–Wilson approximation. The approximation fails when the system possesses a long-range order shown by the coherent Bragg peak. In numerical calculations, the presence of long-range order can be traced by calculating the Debye–Waller factor. When it is less than 10^{-3}, the effect of long-range order on the diffraction profiles is negligible. With increasing reflection order, the Debye–Waller factor decreases, and the applicability of the Stokes–Wilson approximation improves. Hence, this approximation can be applied to higher-order reflections even when it is not applicable for low reflection orders.

This work has been funded by Deutsche Forschungsgemeinschaft (DFG) grant KA 3262/2-2 and the Russian Science Foundation grant 14-11-00083.

References

Balogh, L., Capolungo, L. & Tomé, C. N. (2012). *Acta Mater.* **60**, 1467–1477.
Chandrasekhar, S. (1943). *Rev. Mod. Phys.* **15**, 1–89.
Chavanis, P.-H. (2009). *Eur. Phys. J. B*, **70**, 413–433.
Chavanis, P.-H. & Sire, C. (2000). *Phys. Rev. E*, **62**, 490–506.
Csikor, F. F. & Groma, I. (2004). *Phys. Rev. B*, **70**, 064106.
Groma, I. (1998). *Phys. Rev. B*, **57**, 7535–7542.
Groma, I. & Bakó, B. (1998). *Phys. Rev. B*, **58**, 2969–2974.
Groma, I. & Monnet, G. (2002). *J. Appl. Cryst.* **35**, 589–593.
Groma, I., Ungár, T. & Wilkens, M. (1988). *J. Appl. Cryst.* **21**, 47–53.
Holtsmark, J. (1919). *Ann. Phys. (Leipzig)*, **58**, 577–630.
Kaganer, V. M., Brandt, O., Trampert, A. & Ploog, K. H. (2005). *Phys. Rev. B*, **72**, 045423.
Kaganer, V. M., Köhler, R., Schmidbauer, M., Opitz, R. & Jenichen, B. (1997). *Phys. Rev. B*, **55**, 1793–1810.
Kaganer, V. M. & Sabelfeld, K. K. (2009). *Phys. Rev. B*, **80**, 184105.
Kaganer, V. M. & Sabelfeld, K. K. (2010). *Acta Cryst.* A**66**, 703–716.
Kamminga, J.-D. & Delhez, R. (2000). *J. Appl. Cryst.* **33**, 1122–1127.
Krivoglaz, M. A. (1961). *Fiz. Met. Metalloved.* **12**, 465–475.
Krivoglaz, M. A. (1996). *X-Ray and Neutron Diffraction in Nonideal Crystals.* Berlin: Springer.
Krivoglaz, M. A. & Ryaboshapka, K. P. (1963). *Fiz. Met. Metalloved.* **15**, 18–31.
Landau, L. D. & Lifshitz, E. M. (1970). *Theory of Elasticity.* Oxford: Pergamon Press.
Leineweber, A. & Mittemeijer, E. J. (2010). *J. Appl. Cryst.* **43**, 981–989.
Leoni, M., Martinez-Garcia, J. & Scardi, P. (2007). *J. Appl. Cryst.* **40**, 719–724.
Levine, L. E. & Thomson, R. (1997). *Acta Cryst.* A**53**, 590–602.
McKeehan, M. & Warren, B. E. (1953). *J. Appl. Phys.* **24**, 52–56.
Martinez-Garcia, J., Leoni, M. & Scardi, P. (2009). *Acta Cryst.* A**65**, 109–119.
Min, I. A., Mezić, I. & Leonard, A. (1996). *Phys. Fluids*, **8**, 1169–1180.
Ribárik, G., Ungár, T. & Gubicza, J. (2001). *J. Appl. Cryst.* **34**, 669–676.
Rytov, S. M., Kravtsov, Y. A. & Tatarskii, V. I. (1988). *Principles of Statistical Radiophysics 2: Correlation Theory of Random Processes.* Berlin: Springer.
Scardi, P. & Leoni, M. (2002). *Acta Cryst.* A**58**, 190–200.
Sornette, D. (2006). *Critical Phenomena in Natural Sciences.* Berlin: Springer.
Stokes, A. R. & Wilson, A. J. C. (1944). *Proc. Phys. Soc. London*, **56**, 174–181.

Strunin, B. M. (1967). *Fiz. Tverd. Tela*, **9**, 805–812.
Ungár, T., Groma, I. & Wilkens, M. (1989). *J. Appl. Cryst.* **22**, 26–34.
Upadhyay, M. V., Capolungo, L. & Balogh, L. (2014). *J. Appl. Cryst.* **47**, 861–878.
Warren, B. E. (1959). *Prog. Met. Phys.* **8**, 147–202.
Warren, B. E. (1969). *X-ray Diffraction.* Reading, MA: Addison–Wesley.
Warren, B. E. & Averbach, B. L. (1950). *J. Appl. Phys.* **21**, 595–599.
Warren, B. E. & Averbach, B. L. (1952). *J. Appl. Phys.* **23**, 497–498.
Wilkens, M. (1963). *Phys. Status Solidi*, **3**, 1718–1737.
Wilkens, M. (1970*a*). *Phys. Status Solidi A*, **2**, 359–370.
Wilkens, M. (1970*b*). *Fundamental Aspects of Dislocation Theory*, edited by J. A. Simmons, R. de Wit & R. Bullough, pp. 1195–1221. Washington: US National Bureau of Standards, Special Publication.
Wilkens, M. (1976). *Krist. Tech.* **11**, 1159–1169.
Wilson, A. J. C. (1955). *Nuovo Cimento*, **1**, 277–283.
Zasimchuk, E. E. & Selitser, S. I. (1984). *Fiz. Tverd. Tela*, **26**, 1148–1150.